Available online at www.sciencedirect.com
ScienceDirect
Journal of Catalysis 254 (2008) 310–324
JOURNAL OF CATALYSIS
www.elsevier.com/locate/jcat

Mesoporous Co_3O_4–CeO_2 and Pd/Co_3O_4–CeO_2 catalysts: Synthesis, characterization and mechanistic study of their catalytic properties for low-temperature CO oxidation

Jin-Yong Luo [a], Ming Meng [a,*], Xiang Li [a], Xin-Gang Li [a], Yu-Qing Zha [a], Tian-Dou Hu [b], Ya-Ning Xie [b], Jing Zhang [b]

[a] *Department of Catalysis Science & Technology, School of Chemical Engineering and Technology, Tianjin University, Tianjin 300072, PR China*
[b] *Institute of High Energy Physics, Chinese Academy of Sciences, Beijing 100049, PR China*

Received 2 August 2007; revised 17 October 2007; accepted 4 January 2008

Available online 7 February 2008

Abstract

Several nanosized catalysts Co_3O_4–CeO_2 with varying compositions were synthesized by a surfactant-template method and further promoted by a small amount of Pd (0.5 wt%). These catalysts exhibit uniform mesoporous structure and high surface area (>100 $m^2\,g^{-1}$). The Co_3O_4 crystallites in these catalysts are encapsulated by nanosized CeO_2 with only a small fraction of Co ions exposing on the surface and strongly interacting with CeO_2. Such structure maximizes the interaction between Co_3O_4 and CeO_2 in three dimensions, resulting in unique redox properties. The introduction of Pd prominently enhances both the reduction and oxidation performance of the catalysts, due to hydrogen or oxygen spillover. These catalysts prepared by surfactant-template method exhibit excellent oxidation performance, especially the ones promoted with Pd, which show markedly enhanced CO oxidation activity even at room temperature. Based upon the results of structural properties, redox behaviors and *in situ* DRIFTS study, two different reaction pathways over Co_3O_4–CeO_2 and Pd/Co_3O_4–CeO_2 are proposed.

Keywords: Cobalt oxide; Ceria; Palladium; Mesoporous catalyst; CO oxidation; Structural characterization; Synergy; Mechanism

1. Introduction

Carbon monoxide (CO) is one of the main gaseous pollutants, which is generally produced and released from the combustion process of fossil fuel. For instance, during the cold start period of vehicles, a lot of carbon monoxide (CO) and hydrocarbons (HCs) are generated because of the incomplete combustion of fuel. At the moment, since the temperatures of emission and catalyst bed are very low, the three-way catalysts (TWCs) exhibit poor catalytic oxidation performance, which results in the release of a considerable fraction (50–80%) of emission into the air [1]. Therefore, it is highly necessary to explore low-temperature oxidation catalysts for the removal of CO and HCs. Recently, much attention has been attracted to the cobalt oxide catalysts (Co_3O_4, Co_3O_4/Al_2O_3) due to their unique activity for ambient CO oxidation [2,3]. It is reported that the light-off temperature (T_{50}) for CO oxidation over Co-based catalysts is as low as −63 °C [4]. Cerium oxide, as oxygen storage material, is often added to TWCs, since it not only possesses high oxygen storage capacity (OSC), but also enhances and stabilizes the dispersion of transition metal oxides. Consequently, it is feasible to develop oxidation catalysts mainly consisting of cobalt and cerium oxides.

As catalysts, Co–Ce mixed oxides have been applied in many reactions, such as low-temperature CO oxidation [5,6], methanol oxidation [7], CH_4 combustion [8,9], diesel soot oxidation [10], N_2O decomposition [11] and Fischer–Tropsch synthesis [12]. During these reactions, a catalytic synergistic effect between cobalt and cerium oxides is observed, especially for the oxidation reaction. It is well established that the preparation method could exert a basic influence on the structural properties of the catalysts, like surface area, component dispersion and

* Corresponding author. Fax: +86 22 2740 5243.
E-mail address: mengm@tju.edu.cn (M. Meng).

0021-9517/$ – see front matter
doi:10.1016/j.jcat.2008.01.007

strength of interaction, which in turn determines the redox properties and reactivity of the final catalysts. Recently, by using surfactant cetyltrimethyl ammonium bromide (CTAB) as template, our group has successfully synthesized mesoporous La–Co–Ce–O and La–Co–Zr–O with large surface areas [13,14]. By using the same template, CuO–CeO_2 binary catalysts with high surface area have also been synthesized [15]. Due to the existence of more reactive sites, these catalysts show high catalytic activity for CO oxidation.

Moreover, it is believed that the oxidation activity of base metal oxide catalysts can be prominently enhanced by the addition of a small amount of Pd, sometimes to a great extent, which is called active-phase enhancement (APE) [16]. Nowadays, more and more studies are focusing on the catalysts with combination of noble metal and base metal oxides for oxidation applications, like Pd–(Cr, Cu)/(Ce, Zr)O_x/Al_2O_3 [17,18], Pt–(MnO_x, CoO_x)/SiO_2 [19], Co–(Pt, Pd, Rh)/Ce–Al–O(Al_2O_3) [20], Pd–(Fe, Mn, Co, Ni, Cu)–O_x/NaZSM-5 [21], Pd/(Mn_2O_3 + SnO_2) [22], and Pd(–Pt)/Co_3O_4(Co_3O_4–CeO_2) [23–26]. For CO oxidation, most researchers believe that noble metal is responsible for CO adsorption and base metal oxide for oxygen supply. The spillover of CO from noble metals to base metal oxides is a potential interpretation for the enhancement effect.

In this work, a series of mesostructured catalysts Co_3O_4–CeO_2 with high surface area were prepared by using a surfactant-template method, even with Co/(Co + Ce) atomic ratio up to 40%. These catalysts exhibit quite unique redox properties of cobalt phase, such as the low-temperature initiation for its reduction and oxidation, and especially the high-temperature extending for reduction completion. For CO oxidation, these catalysts display a volcano-type behavior as Co_3O_4 content increases. The catalyst with the best oxidation performance is further promoted by a small amount of palladium, and a remarkably improved CO oxidation activity is achieved even at room temperature (RT), compared with those of Co_3O_4–CeO_2 and Pd/CeO_2. The unique properties and the synergy effect between Pd and Co_3O_4–CeO_2 are interpreted in terms of structural information derived from physicochemical analysis. A novel pathway for CO oxidation over Pd/Co_3O_4–CeO_2 is proposed, which is quite different from the generally-believed one that noble metal is responsible for CO adsorption and base metal oxide, like Co_3O_4 and CeO_2, for oxygen supply.

2. Experimental

2.1. Catalyst preparation

The Co_3O_4–CeO_2 catalysts with different Co/(Co + Ce) atomic ratios (15%, 20%, 30%, 40%), denoted as CeCo15, CeCo20, CeCo30 and CeCo40, respectively, were prepared by surfactant-template method using CTAB (Fuchen Chemical Reagents Factory) as template. Appropriate amounts of $CoCl_2{\cdot}6H_2O$, $CeCl_3{\cdot}7H_2O$ (Shanghai Chemical Reagents Factory) and CTAB were dissolved in distilled water at room temperature and stirred for 15 min, then NaOH solution (2 M) was added slowly to the above solution under vigorous stirring until pH arrived at ca. 11. After stirring for 2 h, the obtained brown suspension was transferred to a Teflon-sealed autoclave and aged at 120 °C for 48 h. The obtained precipitate was filtered and washed, first with water and then with acetone in order to remove the surfactant thoroughly. The resulting black powder was dried at room temperature and calcined in air at 500 °C for 4 h. Then part of the CeCo30 catalyst was impregnated in the aqueous solution of $Pd(NO_3)_2$, giving a Pd loading of 0.5 wt%. The obtained precursor was then dried at 120 °C and calcined in air at 500 °C for 1 h. All these catalysts prepared by the surfactant-template method are denoted as ST catalysts.

For comparison, 0.5 wt% Pd/CeO_2 catalyst was also prepared by impregnating CeO_2 powder into aqueous solution of $Pd(NO_3)_2$. The support CeO_2 was prepared by thermal decomposition of $Ce(NO_3)_3{\cdot}6H_2O$ at 600 °C for 4 h (S_{BET} = 50.4 $m^2\,g^{-1}$). After drying at 120 °C overnight, the solid was calcined in air at 500 °C for 4 h.

In addition, a series of Co_3O_4–CeO_2 catalysts with Co/(Co + Ce) ratio of 0.2 were also prepared by co-precipitation, impregnation and combustion. The co-precipitated sample, denoted as CeCo20-CP, was synthesized by dropwise addition of NaOH (2 M) to a mixed solution of $CoCl_2{\cdot}6H_2O$ and $CeCl_3{\cdot}7H_2O$ at room temperature under vigorous stirring until pH arrived at ca. 11. After stirring for 2 h, the obtained precipitate was filtered and washed with distilled water until no Cl^- ions in the filtrate could be detected by $AgNO_3$. The sample synthesized by combustion, denoted as CeCo20-CB, was prepared by introducing a minimum volume of mixed solution of $Co(NO_3)_2{\cdot}6H_2O$, $Ce(NO_3)_3{\cdot}6H_2O$ and urea (molar ratio: urea/nitrate = 4) into an open muffle furnace, preheated at 400 °C. The solution was boiling and then burning, yielding a foamy, voluminous black powder catalyst. For the impregnation sample, denoted as CeCo20-IM, it was prepared by immersing CeO_2 powder (S_{BET} = 50.4 $m^2\,g^{-1}$) into aqueous solution of $Co(NO_3)_2{\cdot}6H_2O$. All the precursors of above catalysts were dried at 120 °C and calcined in air at 500 °C for 4 h to obtain the final catalysts.

2.2. Evaluation of catalytic activity

The evaluation of catalytic activity of the catalysts was carried out in a continuous fixed-bed quartz tubular reactor (i.d. 8 mm) mounted in a tube furnace. The reaction temperature was measured by putting a thermo-couple in the middle of catalyst bed. The feed and product mixtures were analyzed by a gas chromatograph (BFS SP-3430) equipped with thermal conductivity and flame ionization detectors. The feed gas mixture consisting of 1 vol% CO, 5 vol% O_2 and balance N_2 was led over the catalyst (600 mg) at a flow rate of 100 ml min^{-1}, equivalent to a weight hourly space velocity (WHSV) of 10 000 ml g^{-1} h^{-1}.

2.3. Catalyst characterization

Surface area, pore volume and pore size distribution were measured by nitrogen adsorption/desorption at 77 K using a

Quantachrome NOVA-2000 instrument. The samples were degassed at 350 °C for 10 h prior to the adsorption experiments. The surface area (S_{BET}) was determined by BET method in 0–0.3 partial pressure range and the pore size distribution was determined by Barrett–Joyner–Halenda (BJH) method from the desorption branch of the isotherm.

X-ray diffraction measurement was carried out on an X'pert Pro rotatory diffractometer operating at 40 mA and 40 kV using CoK_α as radiation source ($\lambda = 0.17890$ nm). The data of 2θ from 20 to 90° were collected with the stepsize of 0.017°. The average crystallite size of CeO_2 was calculated by using Scherrer equation from the width at half height of line profiles corresponding to crystal plane (1 1 1).

Laser Raman spectra were recorded with a Bruker FS100 FT-Raman spectrometer, equipped with a liquid N_2-cooled super InGaAs detector. The excitation source was the 1064 nm line of a diode pumped YAG laser with the laser power set at 50 mW.

The surface morphology was determined with a Philips XL-30M scanning electron microscope (SEM) instrument operating at 20 kV. TEM and HR-TEM images were obtained using a Philips Tecnai G^2F20 system operating at 200 kV.

Temperature-programmed measurements were performed on a Thermo-Finnigan TPDRO 1100 instrument with a thermal conductivity detector (TCD). Before detection by the TCD, the gas was purified by a trap containing CaO + NaOH materials in order to remove the H_2O and CO_2. A heating rate of 10 °C min^{-1} and a gas flow rate of 20 ml min^{-1} were used. For pure Co_3O_4, the amount of Co is adjusted equivalent to that in CeCo30.

For H_2-TPR test, the quartz tube reactor was loaded with 50 mg sample in powder form and heated from room temperature to 900 °C in 5% H_2/N_2. By replacing the 5% H_2/N_2 with 5% CO/He, CO-TPR tests were also measured.

Prior to TPO test, 50 mg sample was first pre-reduced by the same mixture gas as in H_2-TPR test but heated from room temperature to 600 °C and held for 10 min to ensure a complete reduction. After cooling to room temperature, the reduced sample was heated from room temperature to 900 °C in 6% O_2/He.

Prior to O_2-TPD test, 200 mg sample was pre-heated in pure O_2 from room temperature to 500 °C and held for 30 min. After cooling to room temperature, the sample was heated from room temperature to 900 °C in pure He. The amount of desorbed oxygen was quantified by pulsing known amount of pure oxygen at the end of the test.

X-ray photoelectron spectra (XPS) were recorded with a PHI-1600 ESCA spectrometer using MgK_α radiation (1653.6 eV). The base pressure was 5×10^{-8} Pa. The binding energies were calibrated using C1s peak of contaminant carbon (BE = 284.6 eV) as standard, and quoted with a precision of ±0.2 eV. The surface composition of the samples in terms of atomic ratios was calculated, and Gaussian–Lorentzian and Shirley background were applied for peak analysis.

Extended X-ray absorption fine structure (EXAFS) measurements were carried out on the 1W1B beamline of Beijing Synchrotron Radiation Facility (BSRF) operating at about 120 mA and 2.5 GeV. The absorption spectra of the Co K-edge of samples and reference Co_3O_4 were recorded at room temperature in transmission mode. A Si(111) double-crystal monochromator was used to reduce the harmonic content of the monochrome beam. The back-subtracted EXAFS function was converted into k space and weighted by k^3 in order to compensate for the diminishing amplitude due to the decay of the photoelectron wave. The Fourier transforming of the k^3-weighted EXAFS data was performed in the range of $k = 3.4$ to 14 A^{-1} with a Hanning function window.

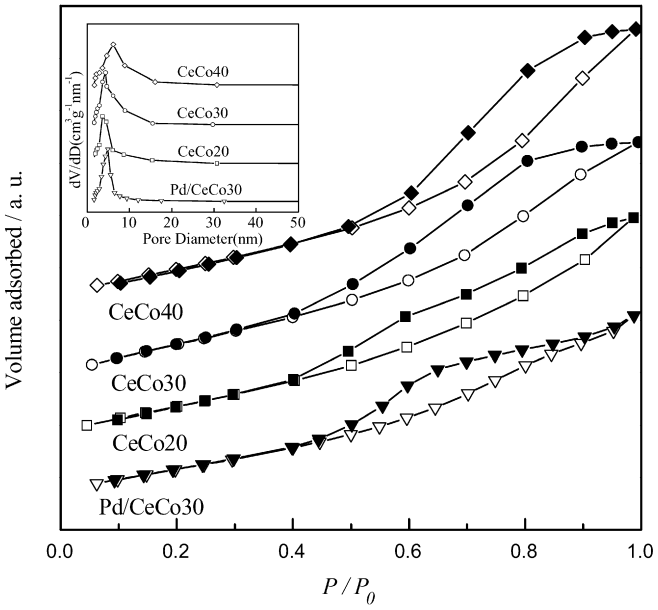

Fig. 1. N_2 adsorption/desorption isotherms of the catalysts (Insert: BJH pore diameter distribution).

In situ diffuse reflectance infrared spectroscopy (DRIFTS) measurement was performed on a Nicolet Nexus spectrometer equipped with a MCT detector cooled by liquid nitrogen, and an *in situ* chamber allowing the sample heated up to 600 °C. Before measurement, the sample powder (30 mg) was treated *in situ* at 300 °C in 6% O_2/He with a flow rate of 50 ml min^{-1} to eliminate water traces. After cooling to room temperature, a background spectrum was collected for spectra correction. Then, 3% CO was introduced to the *in situ* chamber for adsorption. After holding at RT for 20 min, the temperature was increased. The spectra were collected at each temperature, accumulating 32 scans at a resolution of 2 cm^{-1} and displayed in Kubelka–Munk unit.

3. Results and discussion

3.1. Structural properties

The nitrogen adsorption/desorption isotherms are shown in Fig. 1 for the samples prepared by template method. All the samples exhibit typical IV shape isotherms [27], with the P/P_0 position of the inflection point corresponding to a diameter in the mesoporous range. From the BJH pore size distributions inserted in Fig. 1, it can be seen that these samples possess uniform mesoporous structure. The corresponding texture data are

Table 1
Texture data, crystallite size and catalytic activity of the catalysts

Sample	S_{BET} ($m^2\ g^{-1}$)	Pore diameter (nm)	Pore volume ($cm^3\ g^{-1}$)	Crystal-lite size (nm)[a]	T_{50} (°C)[b]
CeCo15	106.9	3.6	0.172	7.0	138
CeCo20	100.0	3.8	0.159	7.1	120
CeCo30	111.9	4.4	0.171	6.0	94
CeCo40	106.3	6.1	0.191	6.2	101
Pd/CeCo30	84.5	4.9	0.130	6.7	58
Pd/CeO_2	60.6	–	–	–	138
CeCo20-CP	79.4	–	–	7.2	127
CeCo20-IM	43.3	–	–	13.2	148
CeCo20-CB	1.7	–	–	37.0	164

[a] Calculated from the line broadening of the d_{111} reflection of CeO_2 using Scherrer equation.
[b] Temperature for 50% conversion for CO oxidation.

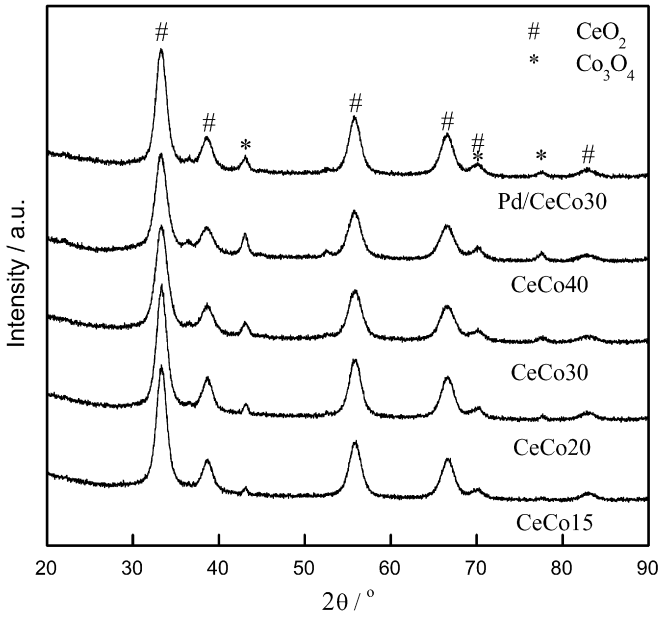

Fig. 2. XRD patterns of the catalysts.

summarized in Table 1. All the four Co_3O_4–CeO_2 ST samples, including that with atomic ratio of Co/(Co + Ce) as high as 40%, show large specific surface area exceeding 100 $m^2\ g^{-1}$, suggesting the effectiveness of this method for the synthesis of mixed oxides possessing high specific surface area. When the atomic ratio of Co/(Co + Ce) is increased from 15% up to 40%, no big difference in specific surface area between all these samples is found, although an obvious increase in pore diameter can be observed. After supported with 0.5 wt% Pd, the specific surface area of Pd/CeCo30 is decreased from 111.9 to 84.5 $m^2\ g^{-1}$, which is possibly due to the partial pore blocking by the introduction of Pd.

Fig. 2 shows the XRD patterns of the Co_3O_4–CeO_2 catalysts. The principal features seen in the diffraction pattern can be ascribed to fluorite oxide CeO_2, with some small peaks typical of Co_3O_4 appearing at ~43 and 77.6°. The CeO_2 crystallite sizes were estimated via CeO_2 (1 1 1) line broadening and the results are listed in Table 1. All the mesostructured samples

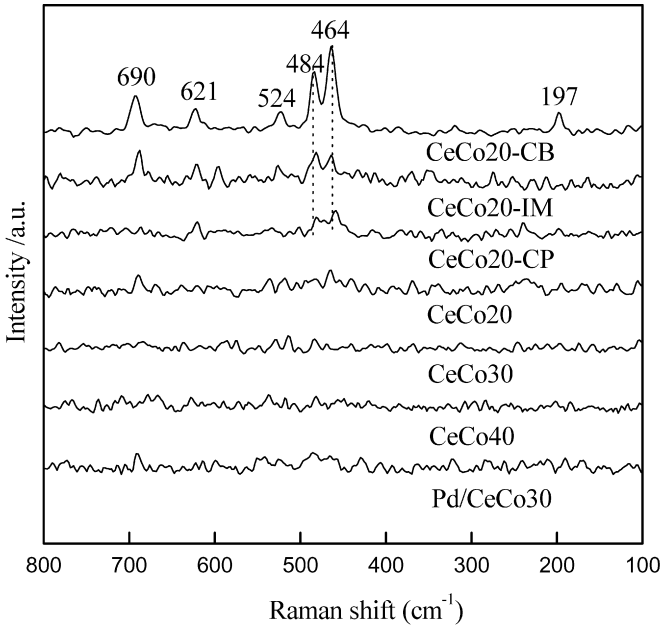

Fig. 3. Raman spectra of the catalysts.

exhibit small crystallite size of CeO_2, among which sample CeCo30 gives the smallest particle size of only 6.0 nm.

Fig. 3 depicts the Raman spectra of the samples under ambient condition. In Fig. 3, the band at 464 cm^{-1} is related to the triply degenerated F_{2g} mode of fluorite CeO_2 [28], and the bands at 197, 484, 524, 621 and 690 cm^{-1} can be assigned to the vibrations of spinel Co_3O_4 [29]. All the samples prepared by combustion, impregnation and co-precipitation display Raman bands of CeO_2 and Co_3O_4, despite the variation in the band intensity. It is rather strange that nearly no active Raman bands can be observed in all the catalysts prepared by template method, although XRD results clearly reveal the diffraction characteristic of CeO_2 and Co_3O_4, which is probably due to the highly defective structure of the catalysts.

From XRD and Raman results, it is difficult to obtain the information about the dispersion state of cobalt species. So, EXAFS measurement was performed. The radial structure functions (RSFs) of Co K-edge of the ST catalysts and standard Co_3O_4 (S_{BET} = 3.3 $m^2\ g^{-1}$), derived from EXAFS, are presented in Fig. 4. The Co environment in Co_3O_4 corresponds to a spinel atomic arrangement with Co^{2+} and Co^{3+} ions located in T_d and O_h coordination. Averagely, each Co atom coordinates with 5.3 O at 0.191 nm (first shell), 4 Co at 0.285 nm (second shell) and 8 Co at 0.336 nm (third shell) [30]. Therefore, in Fig. 4 the first three peaks in the RSF of Co_3O_4 at 0.155, 0.251 and 0.300 nm (not corrected by phase scattering shift), can be assigned to the above three coordination shells. The forth peak at 0.475 nm corresponds to higher Co–Co coordination shell. From Fig. 4, it can be easily found that all the samples display almost identical coordination peaks to Co_3O_4, indicating that the cobalt belongs entirely to Co_3O_4 phase, which is in good agreement with XRD results above. With respect to the peak intensity, it can be clearly seen that the high coordination peaks decrease in the order of Co_3O_4 > CeCo40 > CeCo30 ≅

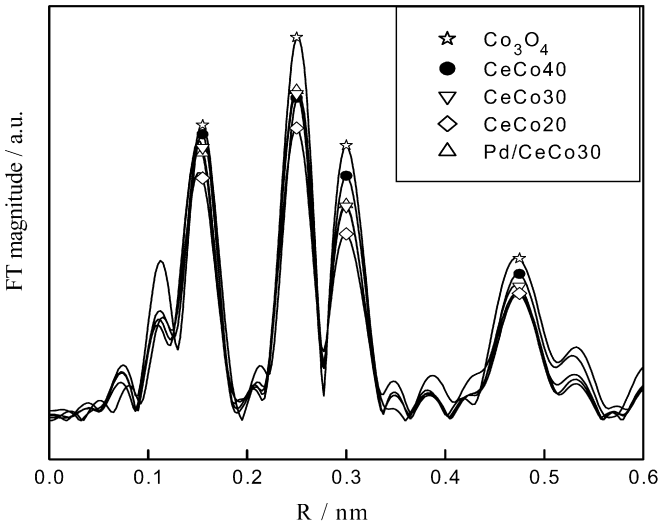

Fig. 4. Co K-edge RSFs of the catalysts.

Pd/CeCo30 > CeCo20. Generally, the intensity of high coordination peaks provides a direct indication of the crystallization degree of the corresponding metal or oxides [31,32]. On this basis, it can be deduced that the Co_3O_4 particle size increases with the elevation of cobalt content. After deposition of Pd on CeCo30, the agglomeration of CeO_2 particles is observed (see Table 1), however, little change in the average particle size of Co_3O_4 is found.

The morphological properties of the catalysts are investigated by SEM and TEM as shown in Figs. 5 and 6, respectively. From the SEM images in Fig. 5, it can be seen that the CeCo30 sample features a shaggy surface, composed of small crumb-like particles with a large degree of porosity, and deposition of Pd induces surface aggregation to some extent. From the low-magnification TEM images presented in Figs. 6a and 6b, it is clear that both catalysts display surface agglomeration of nanoparticles with uniform size distribution. The Pd-promoted sample shows larger particle size than the unpromoted one. However, no well-defined mesoporous structure, like those in Si-containing molecular sieves, could be observed in all these ST catalysts, suggesting that these meso-pores with uniform size are randomly distributed among a mixture of small nanoparticles. The morphology of the nanoparticles has been analyzed by high-resolution TEM, as indicated in Figs. 6a′ and 6b′. These samples are revealed to be assembled by randomly oriented spherical nano-crystallites. The most frequently observed reflection with d spacing value of 0.31 nm corresponds to crystal lattice plane (1 1 1) of CeO_2. The reflection with spacing value of 0.27 nm, attributable to the lattice plane (2 0 0) of fluorite CeO_2, can also be identified.

3.2. Redox behaviors

3.2.1. H_2-TPR profiles and cobalt phase dispersion

The H_2-TPR profiles of CeO_2, Co_3O_4 and samples CeCo20 prepared by different methods are displayed in Fig. 7a and those ST catalysts are shown in Fig. 7b. Pure CeO_2 shows two reduction peaks, one at 528 °C, attributed to the reduction of surface

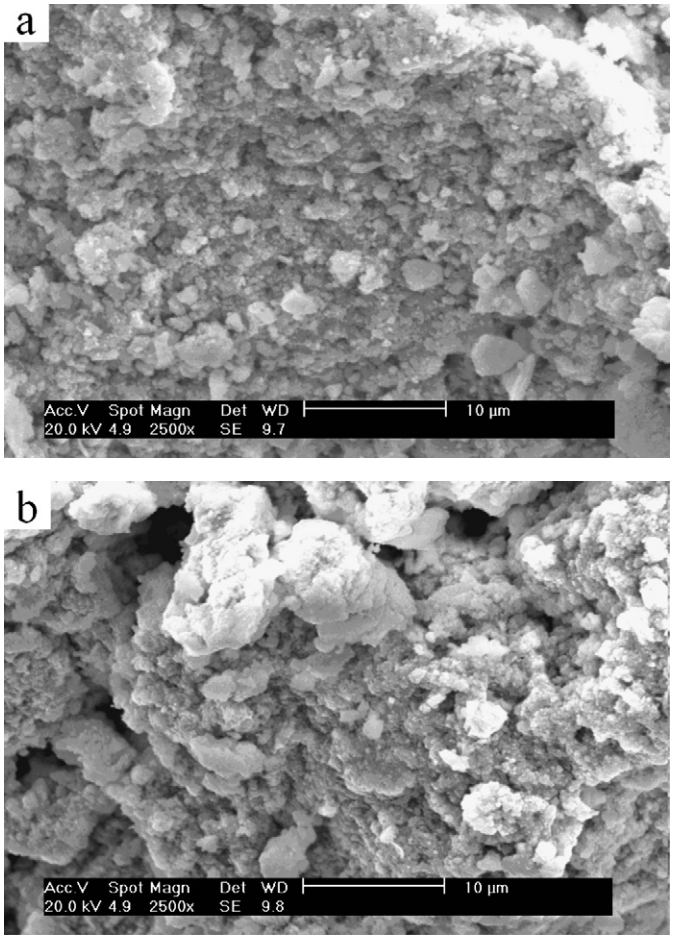

Fig. 5. SEM images of the catalysts: (a) CeCo30, (b) Pd/CeCo30.

oxygen species (capping oxygen), and the other at 820 °C, due to the reduction of bulk oxygen [33]. All the samples display a peak at 820 °C due to the bulk CeO_2 reduction, and the reduction peaks below this temperature are mainly related to Co_3O_4 phase because cobalt species have a much higher reducibility, as compared with CeO_2. In addition, the surface reduction of CeO_2 normally consumes much less H_2, which could be overlapped by the reduction of cobalt species.

With respect to the reduction steps of Co_3O_4, it is rather controversial in literature. Arnoldy and Moulijn [34] observed a single step for the reduction of Co_3O_4, while many others [5,6,8,11] reported that the reduction of Co_3O_4 is a two-step process, involving in the reduction to CoO. The results here clearly show that the reduction behaviors of Co_3O_4 strongly depend on preparation, catalyst composition and dispersion behavior, consistent with the finding of Spadaro et al. [12]. Large particles of Co_3O_4 are often reduced directly to metallic Co in a single step, while fine particles of Co_3O_4 that interact with ceria seem to get reduced in two steps. The first step is generally promoted by component interaction between them, possibly ascribed to the lengthening in the Co–O bond, while the second step is perhaps delayed by the stabilization effect of ceria to cobalt ions at medium valence, similar assignment has ever reported by Martínez-Arias et al. for CuO/CeO_2 system [35]. On

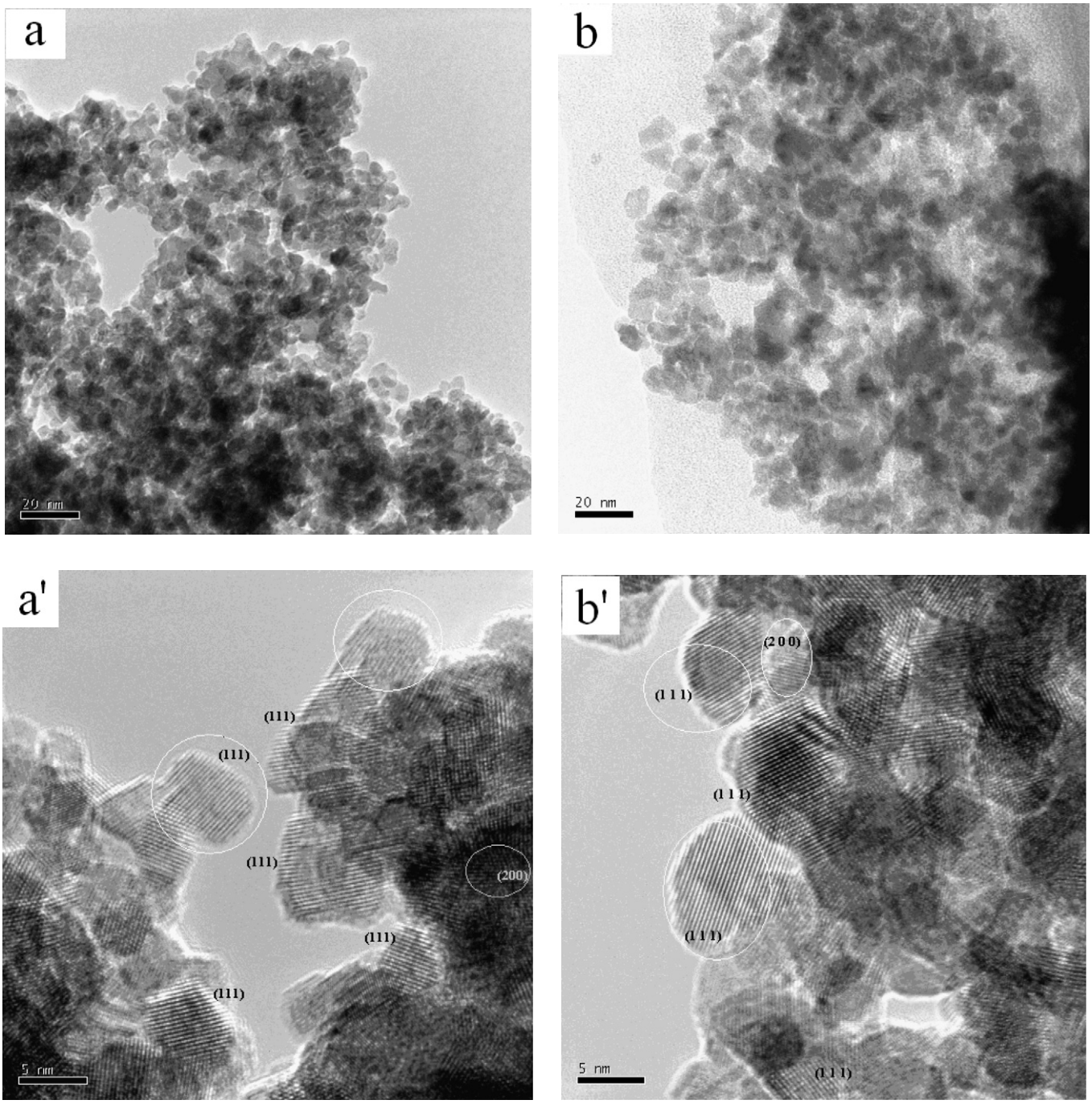

Fig. 6. TEM and HR-TEM images of the catalysts: (a, a′) CeCo30, (b, b′) Pd/CeCo30.

this basis, the following assignments are made for the reduction of cobalt species in respect of the temperature range:

Range A (below 240 °C): reduction of the surface adsorbed oxygen species (indicated as peak α for the ST catalysts);

Range B (240–320 °C): reduction of Co^{3+} at the interface between Co_3O_4 and CeO_2 to Co^{2+} (peak β);

Range C (320–480 °C): reduction of independent Co_3O_4 that weakly interacts with CeO_2 directly to Co (peak γ);

Range D (480–700 °C): reduction of Co^{2+} interacting with CeO_2 to Co (peak θ).

Since the peaks in range C are related to independent or bulk-like Co_3O_4 phase, it is probable to infer the dispersion state of Co_3O_4 phase from the intensity of this peak. Therefore, as shown in Fig. 7a, the dispersion of Co_3O_4 in different catalysts can be ordered as CeCo20 > CeCo20-CP > CeCo20-IM > CeCo20-CB, which is in good agreement with the results of surface area and EXAFS analysis (see Supporting Fig. S1). Thus it can be seen that the preparation method has significant effect on the component dispersion. For all the catalysts prepared by template method, as shown in Fig. 7b, only very small peaks corresponding to independent Co_3O_4 can be observed, even for the catalyst with high cobalt content, suggesting high component dispersion in these catalysts. It should be noted that no obvious reduction peak of indepen-

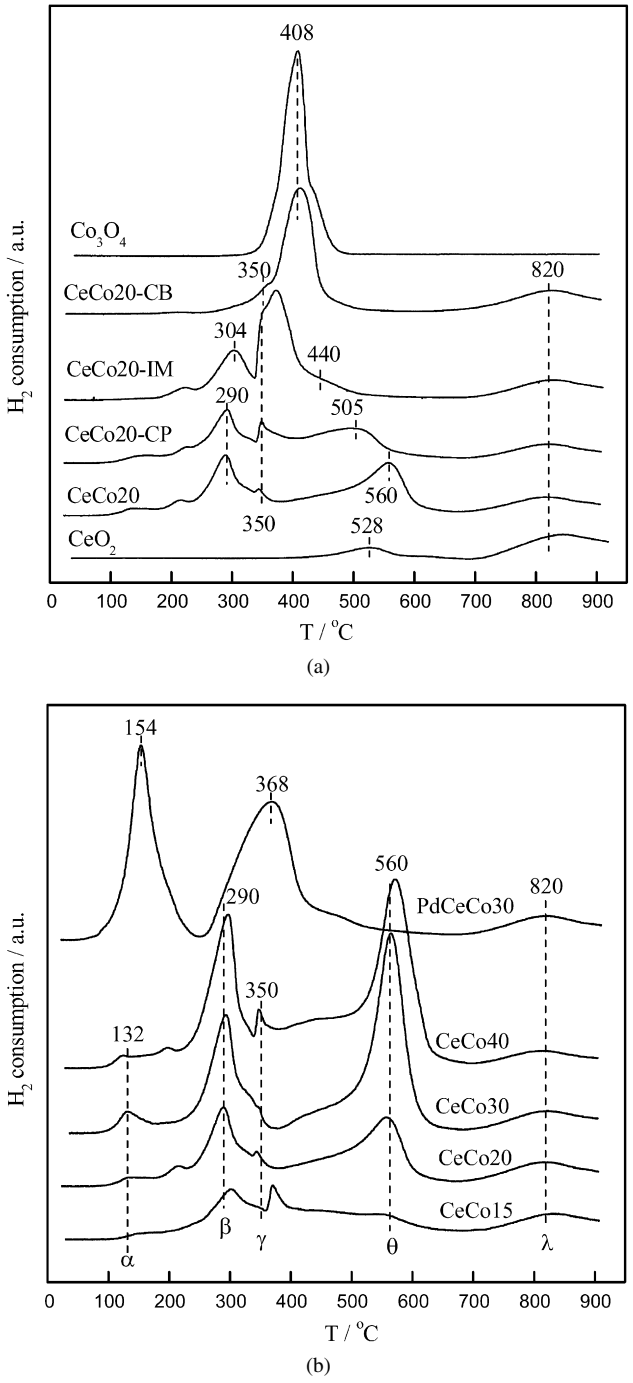

Fig. 7. H_2-TPR profiles of the catalysts: (a) CeCo20 prepared by different methods, Co_3O_4 and CeO_2, (b) catalysts prepared by the surfactant-template method.

dent Co_3O_4 can be observed for catalyst CeCo30, implying that almost all the cobalt species share a homogeneous interaction with CeO_2 phase. A rather large and sharp reduction peak for Co^{2+} interacting with CeO_2 may put further evidence on this homogeneous interaction. This homogeneous and profound interaction can provide the largest Co_3O_4–CeO_2 interface area, therefore, the sample CeCo30 should contain the largest amount of adsorbed surface oxygen, as verified by the largest area of peak α.

3.2.2. Hydrogen spillover and implying structure

A phenomenon worthy of note in H_2-TPR is that for CeCo20 catalysts prepared by different methods, with the amount of independent Co_3O_4 increasing, not only the amount of Co^{2+} ions interacting with CeO_2 is decreased, but their reduction shifts to lower temperature, as shown in Fig. 7a. This temperature shift could be ascribed to hydrogen spillover. Once small amount of the independent Co_3O_4 is reduced directly to metallic Co, this phase will serve as catalyst triggering the reduction of the remaining phase by dissociating H_2. Therefore, the larger amount of the independent Co_3O_4 exists, the more hydrogen atoms are generated, as a result, the subsequent reduction process can be promoted to a greater extent, giving lower reduction temperature. Such a hydrogen spillover is thought to be commonly present in H_2-TPR process [15]. The essential of it can be considered as a self-catalysis or self-acceleration of the gas (H_2)–solid reaction. Due to spillover effect, pure Co_3O_4 is reduced quickly in one step with a sharp peak in H_2-TPR profile. In the same way, for Co_3O_4–CeO_2 systems, the reduction of Co^{2+} interacting with CeO_2 can be also promoted by some exposed metallic Co. Therefore, hydrogen spillover shifts the reduction of interacted cobalt phase towards lower temperatures. Sometimes, the reduction of independent Co_3O_4 and the remaining interacted phase is even overlapped in a single peak, such as in CeCo20-IM and CeCo20-CB samples studied here. This should be a reasonable interpretation for the observation by many researchers that the reduction of Co_3O_4 phase is a two-step process via intermediate CoO, but the ratio of the peak area is generally smaller than the stoichiometric ratio 1:3, even to a great extent sometimes [5,6,8,11]. With respect to the ST samples studied here, peak θ does not seem to be proportional to peak β, especially for sample CoCe15 as shown in Fig. 7b. It seems that peak β is larger, which is resulted from the ceria reduction overlapped with the reduction of Co^{3+} to Co^{2+}, the ceria reduction is here promoted by the interaction between cobalt oxide and ceria. This phenomenon is more obvious for samples with low cobalt content and high surface area, since the reduction of ceria is more evident. In literature [8] it is also found that the excess amount of hydrogen is required for the reduction of Co^{3+} to Co^{2+} in the Co_3O_4–CeO_2 catalysts, which is also due to the reduction of CeO_2.

After promotion with Pd, a more prominent enhancement for the reduction of cobalt species can be observed, as shown in Fig. 7b. The reduction of Co_3O_4 interacting with CeO_2 to CoO takes place only at 154 °C and the consequent reduction of CoO to metallic Co at 368 °C, decreased by 136 and 192 °C, respectively, as compared with the unpromoted Co_3O_4–CeO_2 catalysts. According to literature, structural changes and enhanced oxygen mobility have been proposed to be responsible for the enhanced reduction of base metal oxides, such as in Ag-modified mesoporous manganese oxides [36]. However, with respect to Pd/CeCo30 studied here, the spillover effect should mainly contribute to the enhanced reduction. From the results of CO-TPR as shown in Fig. 8, it can be seen that the samples CeCo30 and Pd/CeCo30 exhibit almost the same reduction pattern. If oxygen mobility was enhanced after deposition of Pd, the reduction by CO would be also promoted in the same

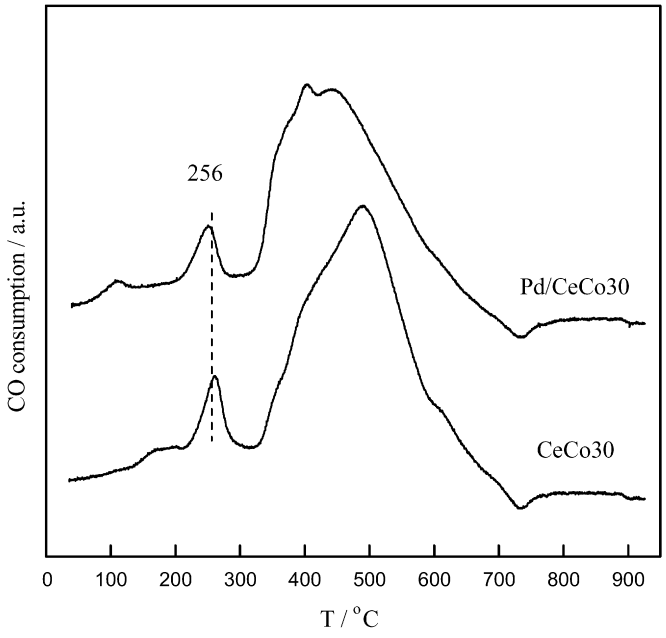

Fig. 8. CO-TPR profiles of CeCo30 and Pd/CeCo30 catalysts.

way as in H_2-TPR. Therefore, hydrogen spillover from palladium to cobalt phase is more likely. It is well known that palladium oxide can be easily reduced to metallic Pd by H_2, and the metallic Pd, as a noble metal, shows intrinsically high capability for hydrogen dissociation, which provides good condition for H_2 spillover. With respect to CO, it is often molecularly chemisorbed on Pd site without dissociation. If the spillover of CO molecule took place, it contributed little to the promotion for the reduction process, since the spilt-over CO molecule is still not activated, totally different from the case for H_2 spillover.

For Co_3O_4–CeO_2 ST catalysts, although some independent Co_3O_4 phase is present, as indicated by the small reduction peak at ∼350 °C, no hydrogen spillover is observed, since all these catalysts exhibit constant reduction temperature as high as 560 °C, which corresponds to the reduction of Co^{2+} to Co. To our knowledge, such high reduction temperature has never been reported for Co_3O_4–CeO_2 or Co_3O_4 systems. Normally, the hydrogen spillover initiates from the surface H_2 dissociation, if there are no exposed metallic atoms on the surface, such as Co, it would be difficult to occur. To make sure the possibility of hydrogen spillover in Co_3O_4–CeO_2 ST catalysts, it is necessary to explore their surface structure.

Table 2 lists the surface Co/(Co + Ce) atomic ratios derived from XPS analysis. The results show that the surface Co/(Co + Ce) ratios are about only half of the nominal one, indicative of a surface Ce enrichment and Co deficiency. While for the Co_3O_4/CeO_2 catalysts prepared by co-precipitation, cobalt enrichment on the surface was observed by Liotta et al. [8]. Hence, the presence of CTAB and hydrothermal aging process may have played an important role for surface Ce enrichment. During preparation, an encapsulation process may have taken place, since the hydrothermal aging process at 120 °C for polymerization/condensation of cerium hydroxyl species possibly induced

Table 2
Surface characterization results from XPS and O_2-TPD

Sample	Co/(Co + Ce)		Ce^{3+}/Ce_{tot}	O_2^{α} ($\mu mol\ g^{-1}$)	O_2^{β} ($\mu mol\ g^{-1}$)
	Nominal	XPS			
CeCo15	0.15	–	–	23.4	48.2
CeCo20	0.2	0.07	0.17	25.3	40.7
CeCo30	0.3	0.13	0.16	37.5	58.0
CeCo40	0.4	0.19	0.15	29.4	59.5
Pd/CeCo30	0.3	0.15	0.13	23.8	27.5

the formation of a thin layer of cerium species on the surface. Similarly, for Pt/CeO_2 prepared by modified microemulsion using CTAB as a cationic surfactant, a total encapsulation structure has also been proposed [37]. The aging process is regarded as the crucial step for the formation of such structure. However, different from the totally encapsulated Pt/CeO_2 catalysts, a small fraction of XPS-detectable Co atoms still exist on the surface for the catalysts studied here, which can be ascribed to the surface migration of Co ions during calcination. It is reported that the calcination process can drive the cobalt from bulk to surface [5]. In this work, since the calcination temperature (500 °C) is not high enough, no bulk Co species are formed on the surface, and only a small fraction of Co exists as surface species, which is believed to be entirely interacting with CeO_2. Therefore, during H_2-TPR process, no or little exposed metallic cobalt is formed because of the absence of independent or bulk cobalt oxides on the surface, and no hydrogen spillover can be observed. Such encapsulation structure maximizes the interaction between cobalt oxide and ceria in three dimensions. As a result, all these ST catalysts show the highest reducibility at low temperature and wide reduction window at high temperature region.

It is hard to distinguish Co^{2+} and Co^{3+} from Co2p spectra due to the small difference in their binding energy value, while the spin–orbit splitting of the 2p peak (ΔE) is found to be well correlated with the oxidation state of Co. It has been reported that a ΔE value of 16.0 eV for cobaltous compounds and 15.0 eV for cobaltic compounds [38]. For the mixed-valence Co_3O_4, a spin–orbit splitting value of 15.2 eV has been reported [39]. Here the spin–orbit value is about 15.4 eV (see Supporting Fig. S2), close to that of Co_3O_4, suggesting that the cobalt species are present mainly as Co_3O_4, as well as some CoO. The relatively intense satellite peak also suggests the presence of CoO, since the high-spin CoO compounds are characterized by an intense shake-up satellite structure, while the mixed-valence oxide Co_3O_4 just shows a weak satellite structure [7]. The presence of CoO is possibly due to the stabilization effect of CeO_2 [7,8]. Fig. 9 presents the experimental and fitted Ce3d spectra of the mesoporous catalysts. The relative concentrations of Ce^{3+} were calculated [40] and listed in Table 2. The uncertainty of the Ce^{3+}/Ce is of the order of 10%. It can be seen that the concentrations of Ce^{3+} on the surface of these catalysts are close to those for Au/$Mn_xCe_{1-x}O_2$ catalysts [40], but larger than those for the reported Co_3O_4–CeO_2 catalysts [8], which implies larger proportion of surface oxygen vacancies. Deposition of Pd decreases the surface oxygen vacancies, which may be attributed to the increased particle size of CeO_2, since the

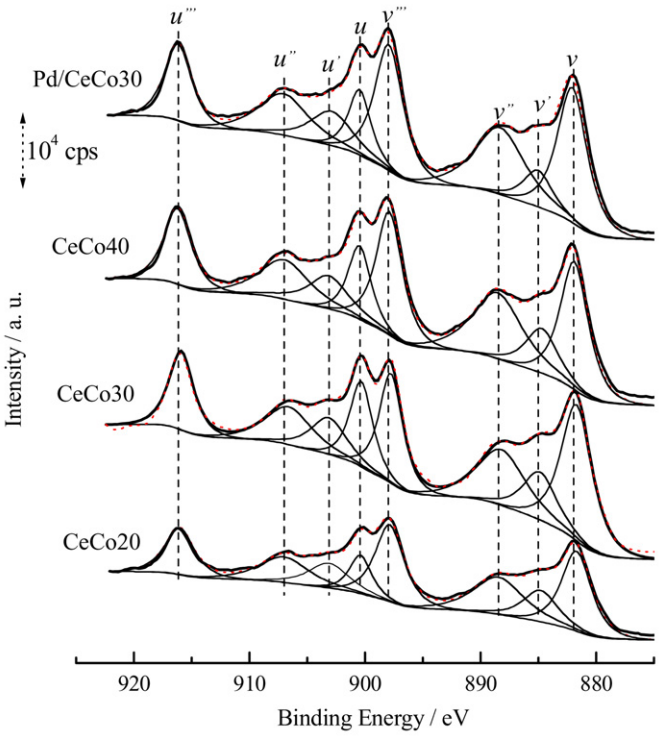

Fig. 9. XPS spectra of Ce3d of the catalysts prepared by the surfactant-template method.

larger particle size corresponds to the smaller amount of exposed Ce^{3+} and the resultant oxygen vacancies [41]. Additionally, from the binding energy band of $Pd3d_{5/2}$ at 336.6 eV, it is found that palladium is present mainly as PdO [24].

3.2.3. TPO, component interaction and oxygen spillover

Before TPO test, the samples were pre-reduced by H_2 (see Experimental section). The TPO profiles for CeO_2, Co_3O_4 and samples CeCo20 prepared by different methods are displayed in Fig. 10a, and those for the ST catalysts are displayed in Fig. 10b. For pure CeO_2, there is nearly no detectable oxygen consumption peak, while for pure Co_3O_4, it is characterized by a broad oxygen consumption peak at 393 °C and a sharp oxygen release peak at 870 °C, due to the oxidation of metallic cobalt to Co_3O_4 and the subsequent thermal decomposition of Co_3O_4 to CoO, respectively [8]. Similar to pure Co_3O_4, all the Co_3O_4–CeO_2 samples exhibit two peaks in their TPO profiles. It should be noted that under inert atmosphere, all the cobalt species decompose at ca. 845 °C (see Supporting Fig. S3 of O_2-TPD in helium flow), regardless of the presence of ceria. Under oxidizing condition, pure Co_3O_4 decomposes at higher temperature of 870 °C, and the presence of ceria further increases the decomposition temperature to 880 °C. Generally, for the decomposition of bulk oxides, the transfer of the bulk oxygen ions to the surface sites takes place first [42,43]. So the presence of surface oxygen vacancies seems to be necessary for bulk oxides decomposition. Under oxidizing condition, the gas phase oxygen may fill the surface oxygen vacancies and decrease the driving force for oxygen diffusion from bulk to surface, in other words, the gas phase oxygen competes with

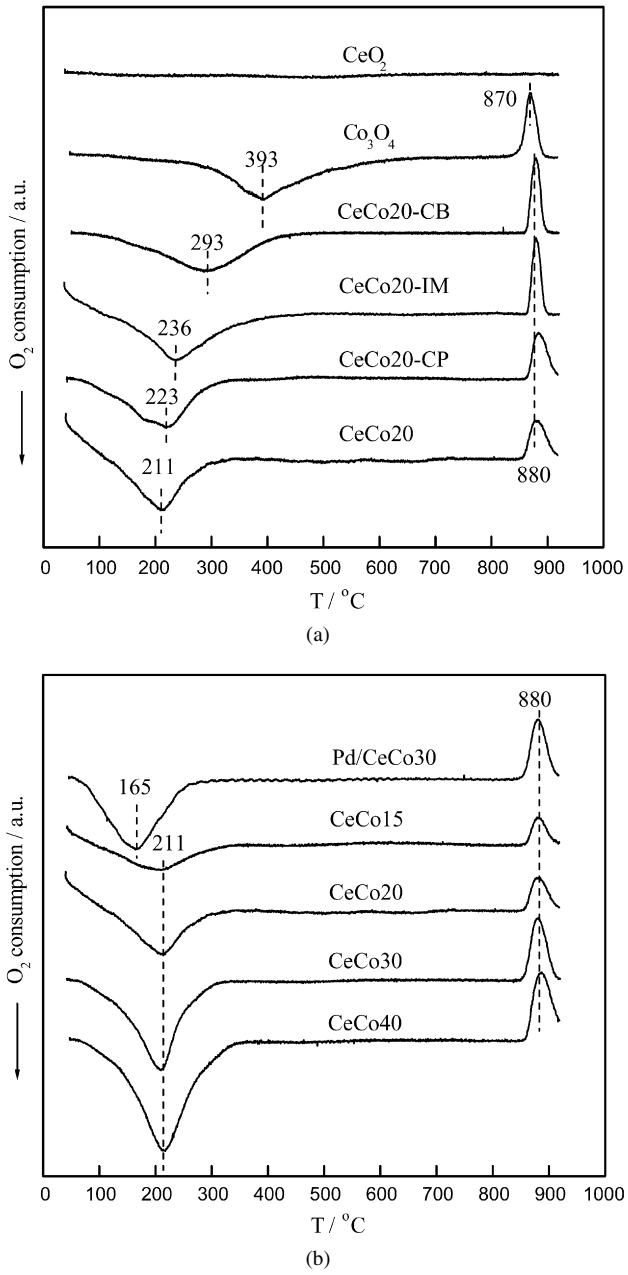

Fig. 10. TPO profiles of the catalysts: (a) CeCo20 prepared by different methods, Co_3O_4 and CeO_2; (b) Catalysts prepared by the surfactant-template method. * Before TPO, samples were pretreated by temperature-programmed reduction under 5% H_2/N_2 at a rate of 10 °C min^{-1} from RT to 600 °C and held for 10 min.

the bulk oxygen for the surface oxygen vacancies, which results in the inhibition of bulk decomposition process. Here, it seems that ceria can trap gas phase oxygen and further increase the surface oxygen concentration due to its well-known oxygen storage capacity. The interaction between CeO_2 and Co_3O_4 perhaps inhibits the thermal decomposition of Co_3O_4 via oxygen supply from CeO_2 to cobalt phase at the interface, leading to the decrease of driving force for oxygen diffusion from bulk to surface. At the same time, it can be seen from Fig. 10a that this interaction also contributes to the easier oxidation of cobalt species. The higher dispersion of cobalt species corresponds

to lower oxidation temperature of metallic Co. Generally, high cobalt dispersion can ensure a more profound contact and interaction between cobalt species and CeO_2, hence facilitating oxygen supply from CeO_2 to cobalt species and promoting the oxidation of cobalt phase.

Since it is widely believed that small particles can decrease diffusion resistance, one may argue that for catalysts prepared by different methods, it is the decrease in the particle size of cobalt that predominantly contributes to the easier oxidation of cobalt species. Indeed, such a decrease in the particle size has been confirmed by EXAFS and TPR results for the catalysts prepared by different methods. But it is considered that the component interaction intrinsically promotes the oxidation of cobalt, rather than the particle size. In former section, the EXAFS results have confirmed the corresponding increase in Co_3O_4 crystallite size for these ST catalysts as cobalt content increases, but all these catalysts exhibit identical temperature at 211 °C for the oxidation of cobalt as shown in Fig. 10b, suggesting that particle size contributes little to the oxidation process. The constant oxidation temperature of Co phase is believed to be associated with the encapsulation structure determined by template method, which maximizes the degree of contact and interaction between Co and cerium species in three dimensions. In contrast, for the co-precipitated Co_3O_4–CeO_2 without encapsulation structure, a variation in the oxidation temperature can be observed as the cobalt loading increases [8]. Furthermore, although CeCo20-CB and pure Co_3O_4 exhibit low surface area (S_{BET}: 1.7 $m^2\,g^{-1}$ for CeCo20 and 3.3 $m^2\,g^{-1}$ for Co_3O_4) and low dispersion of cobalt oxides, a comparison between their oxidation patterns shows that the oxidation temperature of cobalt is lowered almost 100 °C by the co-existence of CeO_2. On this basis, it is considered that the component interaction, which strongly depends on preparation method, intrinsically determines the oxidation patterns of the catalysts.

After Pd deposition, the oxidation of Co is greatly promoted from 211 to 165 °C, decreased by 46 °C. The oxygen spillover is proposed for this promotion. Similar to H_2-TPR, the essential of oxygen spillover can also be considered as a catalytic gas (O_2)–solid (Co) reaction using Pd species as catalyst.

In summary, for Co_3O_4–CeO_2 catalysts prepared by the surfactant-template method, the constant low reduction temperature of Co^{3+} to Co^{2+} and the low oxidation temperature of Co to Co_3O_4, as well as the high reduction temperature for Co^{2+} to metallic Co, indicate a very strong interaction between cobalt and cerium species in these samples, which is closely related to the encapsulation structure. The preparation method is believed to play a crucial role in constructing such a structure. After promotion with Pd, both the reduction and oxidation of cobalt phase are greatly enhanced due to hydrogen or oxygen spillover since palladium is intrinsically active for molecular hydrogen and oxygen dissociation, and the dissociated H or O atoms may be highly mobile and reactive, leading to the easier reduction or oxidation of cobalt phases. From catalytic point of view, the essential of spillover can also be considered as a catalytic gas (H_2, O_2)–solid (Co phase) reaction using Pd as catalyst, leading to the decrease of activation energy.

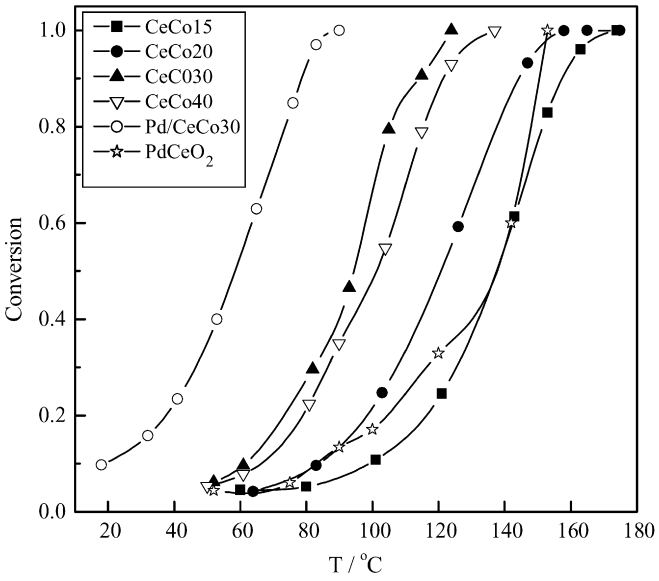

Fig. 11. Light-off curves for CO oxidation over different catalysts. Conditions: 1 vol% CO, 5 vol% O_2 and balance N_2, WHSV = 10 000 ml $g^{-1}\,h^{-1}$.

3.3. Catalytic performance

Fig. 11 shows the catalytic performance for CO oxidation of the Co_3O_4–CeO_2 ST catalysts, as well as Pd/CeO_2 catalyst for comparison. In Table 1, the light-off temperatures of 50% conversion (T_{50}) over different catalysts are listed, including the Co_3O_4–CeO_2 catalysts prepared by different methods. From this table, it can be seen that there are at least three factors that determine the CO oxidation activity, namely the preparation method, cobalt loading and additives/promotion elements. The preparation method mainly determines the surface area, and the higher surface area generally corresponds to higher cobalt dispersion and higher oxidation activity due to more exposed active sites, consistent with the findings of Tang et al. [6]. Among these four preparation methods, the surfactant-template method produces mesoporous Co_3O_4–CeO_2 catalysts with the largest surface area, which exhibit volcano-type oxidation performance for CO oxidation as the atomic ratio of cobalt increases. With the gradual increase of cobalt content to 30%, the active sites increase correspondingly, which results in the promotion in the oxidation activity. While with further increase of cobalt content to 40%, excess cobalt species form bulk Co_3O_4, leading to less profound interaction between Co_3O_4 and CeO_2, which causes the decrease of oxidation activity. The catalyst CeCo30 is the most active one among them with T_{50} only at 94 °C. With the addition of Pd, the CO oxidation activity of the catalyst is enhanced to a great extent. The light-off temperature T_{50} (58 °C) of this catalyst is decreased by 36 °C, as compared with that of the un-promoted one. And catalyst Pd/CeCo30 even shows some oxidation activity at room temperature. By contrast, the activity of Pd/CeO_2 catalyst exhibits light-off temperature T_{50} as high as 138 °C. Although Pd/CeCo30 possesses slightly larger surface area (84.5 $m^2\,g^{-1}$) than Pd/CeO_2 (60.6 $m^2\,g^{-1}$), this small difference would hardly bring such great discrepancies in the catalytic activity. A more

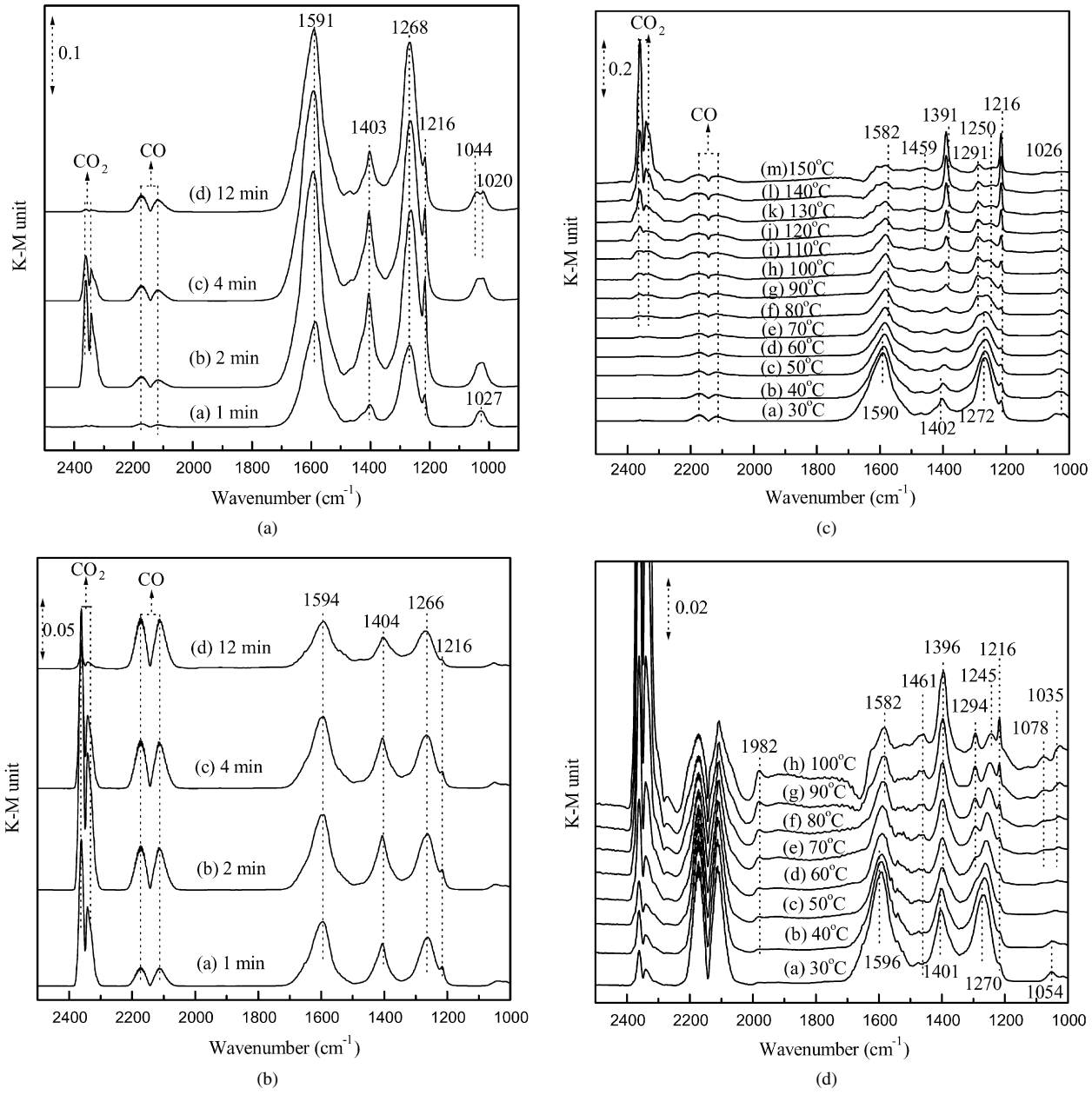

Fig. 12. *In situ* DRIFTS spectra of the catalysts after exposure to CO + O_2: (a) CeCo30 and (b) Pd/CeCo30 at room temperature (25 °C) and different time; (c) CeCo30 and (d) Pd/CeCo30 at different temperatures.

prominent synergism between PdO and Co_3O_4–CeO_2 is believed to be present in Pd/CeCo30 than in Pd/CeO_2.

3.4. *In situ* DRIFTS study

In order to figure out the reason that sample CeCo30 is the most active one among the Co_3O_4–CeO_2 ST catalysts and the synergism essential between PdO and Co_3O_4–CeO_2, *in situ* DRIFTS studies were performed. The results are shown in Fig. 12. For all the samples, the bands in the region of 2300–2400 cm^{-1} are assigned to gaseous CO_2, and the bands in the region of 2050–2200 cm^{-1} are ascribed to CO-related species.

Fig. 12a shows the spectra of CO/O_2 co-adsorption over CeCo30. Upon CO/O_2 admission, strong bands at 1591, 1268 cm^{-1}, as well as a small band at 1027 cm^{-1} are formed first, which could be assigned to surface bidentate carbonate species [44]. Similar bands were also found over pre-oxidized Co_3O_4 upon the co-adsorption of CO + O_2 [3]. Afterwards, strong bands corresponding to gas phase CO_2 (2360 and 2342 cm^{-1}) suddenly appears, suggesting that the ambient CO oxidation over this catalyst has taken place, via surface bidentate carbonates as intermediates. Consequently, surface carbonate species at 1403, 1216 cm^{-1}, due to the adsorption of gas phase CO_2 [3,45] could be observed. After longer exposure, gas phase CO_2 decreases gradually and almost disappears, indicating the decrease in the rate of CO oxidation, but the adsorbed CO_2 species tend to retain on the surface to some extent. Upon heating, these species gradually desorb, as shown in Fig. 12c,

until the temperature is promoted to 70 °C. Above 70 °C, CO oxidation is accelerated again, which is confirmed by the increase of the bands for gaseous CO_2. Meanwhile, the bands due to CO_2 adsorption also increase upon continuous heating. As a result of the surface reaction, bands of bidentate carbonate species originated from CO adsorption decrease, and some of the overlapped bands appear at 1459, 1291 and 1250 cm^{-1}, possibly due to the reversible adsorption of CO_2 [46].

For Pd/CeCo30 catalyst, as shown in Fig. 12b, it exhibits similar spectra to CeCo30. The band positions remain almost unchanged, and the ambient oxidation of CO can also be observed. However, some differences can still be found. Firstly, the intensity of the bidentate carbonate bands decreases to great extent, indicative of the decreased CO adsorption capacity, which is possibly caused by the surface Pd coverage during Pd loading and the decreased surface area due to partial pore blocking. Secondly, the ambient CO oxidation still proceeds even after 12 min exposure, as indicated by the presence of bands corresponding to gaseous CO_2. No band due to CO adsorption on Pd species is found. After heating, the bands of carbonate species similar to CeCo30 could be observed on Pd/CeCo30 catalyst, as shown in Fig. 12d. However, different from the case on CeCo30, the CO oxidation on Pd/CeCo30 is always proceeding, which could be reflected by the continuous presence of gaseous CO_2 and the increase of its band intensity. As CO oxidation proceeds, some metallic Pd can be observed, as verified by the appearing of bridged adsorbed CO on Pd^0 at 1982 cm^{-1}, and the amount of metallic Pd seems to increase with reaction temperature increasing.

3.5. Mechanistic suggestion

From the DRIFTS results, it is found that CO molecule can be easily adsorbed on the surface of Co_3O_4–CeO_2 as bidentate carbonate species, which are the intermediates for CO oxidation. It seems that at least two kinds of oxygen species are present, one is very active and responsible for ambient CO oxidation, and the other is mainly for the oxidation at higher temperature. On this basis, a potential reaction pathway is proposed for CO oxidation over Co_3O_4–CeO_2 ST catalysts, as shown in Fig. 13a.

At first, CO is adsorbed on the surface as bidentate carbonate. The TPR results have confirmed that the Co–O bond at the boundary of Co_3O_4 and CeO_2 breaks up more easily, due to the lengthening of Co–O bond as a result of the component interaction. It can be expected that oxidation takes place preferentially at the interface between surface Co_3O_4 and CeO_2. The adsorbed CO extracts surface oxygen atom at this interface to form CO_2 and surface oxygen vacancy. The CO_2 molecule can adsorb on the surface and further transform into surface carbonate species (bands at 1403, 1216 cm^{-1}), and the oxygen vacancy is filled by gas phase O_2, weakening the bond in O_2 molecule. However, the dissociation of the adsorbed O_2 molecule is endothermic and is not a determining factor to the low-temperature catalytic process [47]. This adsorbed O_2 species, which is believed to be present possibly as O_2^- ion radical [48], may react readily with the neighboring CO molecule adsorbed as bidentate carbonate, forming CO_2 again and recovering the catalyst surface.

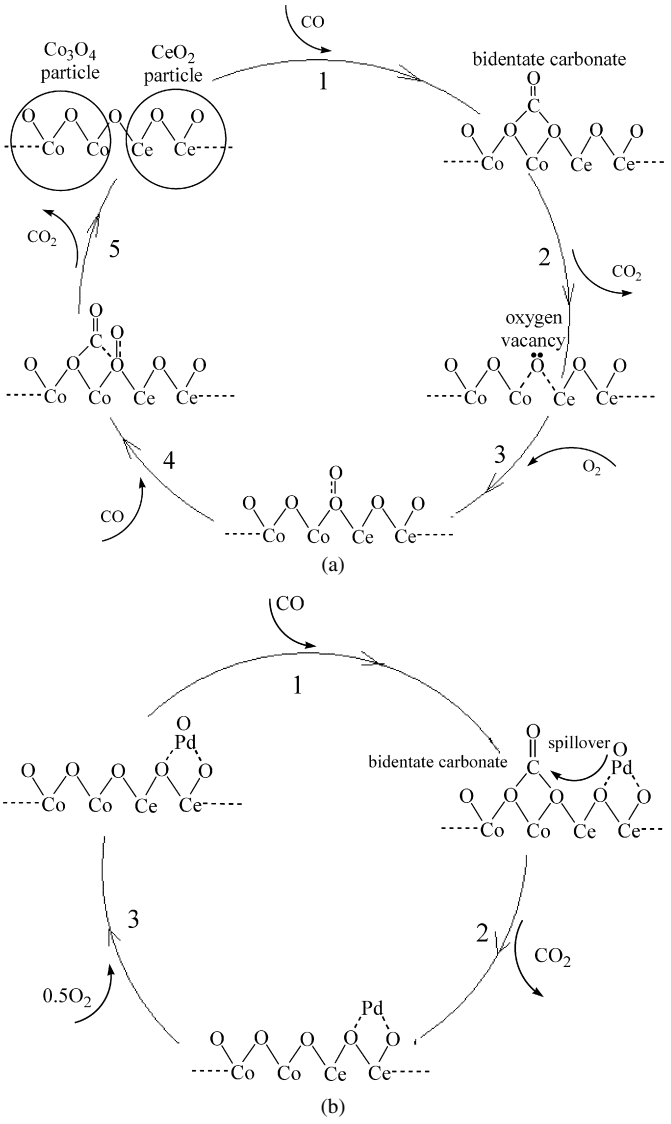

Fig. 13. Proposed CO reaction pathways over the catalysts: (a) CeCo30, (b) Pd/CeCo30.

After O_2/He pretreatment for CeCo30 catalyst, some oxygen species that pre-adsorbed on catalyst surface possibly present as active O_2^- ion radical, which seems to oxidize CO at room-temperature as observed in the DRIFTS spectra. However, the catalyst loses activity due to the depletion of such O_2^- species. It is reported that an oxidation treatment could regenerate the room-temperature activity [3], possibly by supplementing such oxygen species. However, under real reaction condition, the activation of gas-phase oxygen requires the generation of surface oxygen vacancy. The step 2, in which the bidentate carbonate extracts surface lattice oxygen and creates oxygen vacancy, may be the rate-determining step during CO oxidation. This appears to be consistent with the findings by Wang et al. [49], who thought that the rate-determining step for CO oxidation over CuO/SDC is the removal of the surface lattice oxygen of CuO by CO to form oxygen vacancies.

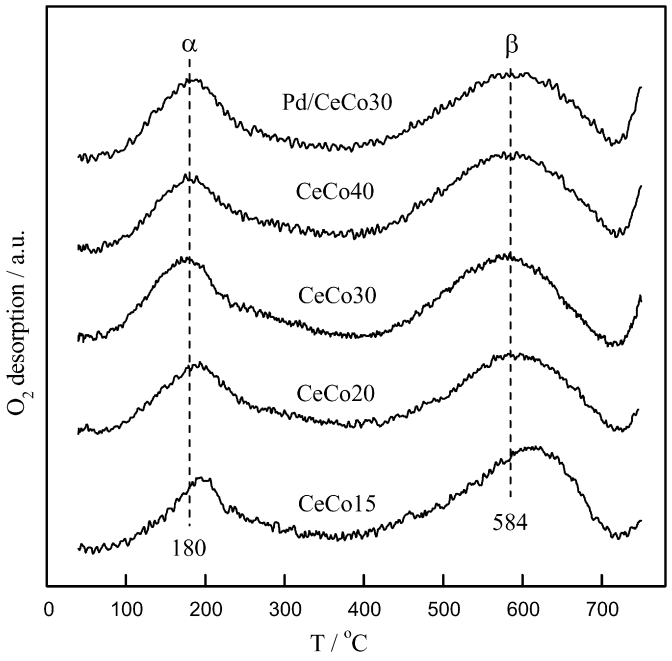

Fig. 14. O_2-TPD profiles of the catalysts prepared by the surfactant-template method. Before O_2-TPD, the samples were pretreated by temperature-programmed oxidation under pure O_2 at a rate of 10 °C min^{-1} from RT to 500 °C and held for 30 min.

Since oxygen vacancies play a crucial role in CO oxidation over Co_3O_4–CeO_2 ST catalysts, a useful technique to study them is temperature programmed desorption of oxygen. Therefore, O_2-TPD measurement was performed and the results are shown in Fig. 14. All these samples exhibit three types of oxygen species, with the peak centered at ca. 180, 584 and 845 °C. Similar to the O_2 release peak during TPO, the very large high-temperature peak at 845 °C corresponds to the thermal decomposition of Co_3O_4 (these peaks are too large and not shown for clarity). The first two small peaks at lower temperature, labeled as α and β, are related to the oxygen evolving from the solid surface. These oxygen species have also been evidenced in Sr- and Ce-doped $LaCoO_3$ systems [50]. With respect to the peak area, the amount of desorbed oxygen was calculated and listed in Table 2.

The high activity of CeCo30 catalyst is understandable since the activity correlates very well with the oxygen species of peak α, namely larger area of peak α corresponds to higher oxidation activity of the catalyst. Sample CeCo30 desorbs the largest amount of oxygen (α), indicating the largest amount of oxygen vacancies in this catalyst. This is also consistent with the TPR results that the largest amount of adsorbed oxygen is reduced in this sample. Since no oxygen is evolved from the surface of pure Co_3O_4 and CeO_2, it is inferred that these oxygen vacancies should present at the interface between Co_3O_4 and CeO_2, possibly due to the interaction between them. On this basis, it is considered that CO oxidation takes place preferentially at the interface between Co_3O_4 and CeO_2. Former TPR results have shown that nearly all the cobalt species share a homogeneous interaction with CeO_2 in CeCo30 sample, which possibly provides the largest interface area. Therefore, this sample displays highest activity among these Co_3O_4–CeO_2 ST catalysts, although the amount of the surface cobalt atoms, which are generally believed to be the active sites, is not the largest in this sample. Our previous study over La–Co–Ce–O systems also demonstrates the importance of interaction between Co_3O_4 and CeO_2, but not of the surface cobalt concentration for CO oxidation [13].

After Pd is loaded on CeCo30, the mechanism pathway in Fig. 13a may not applicable for the interpretation of the ultra high activity of Pd/CeCo30 catalyst, because the amount of the α-oxygen species is decreased, which is possibly due to the partial coverage of Pd, as well as the decreased interface area between Co_3O_4 and CeO_2 due to the slight enhanced crystallization of CeO_2. At the same time, DRIFTS study shows that the CO adsorption ability is lowered to a large degree. All these factors seem to be unfavorable to CO oxidation according to the reaction pathway proposed in Fig. 13a. So, it is believed that the reaction mechanism must have changed over Pd-promoted catalyst, and it seems that a synergism between Pd species and CeCo30 may contribute to the markedly enhanced activity. Keeping in mind that CeCo30 is highly active in CO adsorption and the rate-determining step for CO oxidation is thought to be the creation of oxygen vacancies for oxygen activation, it is natural to assume that Pd species are involved in O_2 activation, since noble metals show intrinsically high ability for oxygen dissociation, even at low temperature. It has been reported that in a bimetallic Fischer–Tropsch catalyst Co–Pd/Al_2O_3, oxygen is continuously dissociated at the metallic Pd phase, which promotes the oxidation of the cobalt phase through oxygen species migration between them even at room temperature (300 K) [51]. On this basis, we thought that oxygen adsorption may be dissociative over Pd/CeCo30, and the dissociated atomic oxygen, which is very mobile and reactive, can spill over through support CeO_2 to the bidentate carbonate sites and readily react. According to above analysis, another CO oxidation pathway over Pd/CeCo30 is proposed and shown in Fig. 13b.

Over CeCo30 the rate-determining step for CO oxidation is the oxidation-assisted creation of oxygen vacancies, while over Pd/CeCo30 no oxygen vacancies are required for CO oxidation as seen in Fig. 13b. The CO molecules adsorbed as bidentate carbonates could be directly oxidized by oxygen species from Pd sites via spillover effect. Such an oxygen spillover process has been confirmed in TPO tests. Actually, our previous study over Pt(Pd, Rh)–Co/Ce–Al–O systems evidenced a common oxygen spillover effect facilitated by even trace amounts of noble metals through the support [20]. During reaction, some metallic Pd exists, which can be observed in DRIFTS study. This metallic phase is possibly responsible for oxygen dissociation. However, in literature [18,22], both the alloy formation and CO spillover have ever been proposed for explanation of the activity enhancement. In the Co_3O_4–CeO_2 ST catalysts studied here, under oxidizing atmosphere and at low temperature, the surface cobalt phase is strongly interacted with CeO_2 and can be hardly reduced to metallic state; therefore, it is not likely to form Pd–Co alloy during CO oxidation. Moreover, it seems difficult for the direct contact between Pd and Co_3O_4 because

of the isolating effect of encapsulation structure. As to the CO spillover from Pd to Co_3O_4–CeO_2, if it takes place, it will contribute little to the activity because the catalyst Co_3O_4–CeO_2, as basic support, is highly capable of adsorbing CO molecules. At the same time, the reverse CO spillover from Co_3O_4–CeO_2 to Pd phase can hardly happen since CO molecules are adsorbed on the surface as relatively stable bidentate carbonates, which possess much lower mobility as compared with atomic oxygen species.

For CO oxidation, Pd/CeCo30 catalyst also shows great advantages, as compared with Pd/CeO_2 catalyst. Although many kinds of preparation methods were applied, the light-off temperature T_{50} over Pd/CeO_2 catalyst is generally higher than 100 °C [52,53], including the results in this work. Based on the results of multi-molecular beam experiments and *in situ* time resolved infrared reflection absorption spectroscopy, Schalow et al. ever [54] found that at low reaction temperature ($T <$ 450 K), the CO oxidation activity of partially oxidized Pd particles is significantly lower than that of metallic Pd particles, due to the weaker CO adsorption on Pd oxide surface. If a pre-reduction treatment is performed, the catalytic activity of Pd/CeO_2 can be improved to some extent [55]. For Co_3O_4–CeO_2 catalysts studied here, the oxidation-assisted creation of oxygen vacancies, as confirmed to be the rate-determining step, proceeds at much higher temperature than RT, limiting the low-temperature oxidation activity of the catalyst. The combination of the basic support CeCo30 with high surface area and large CO adsorption capacity, and noble metal Pd phase decorated on the surface for oxygen activation, exhibits great advantage for low-temperature CO oxidation. Even without any pretreatment, the catalyst Pd/CeCo30 shows excellent CO oxidation activity, holding great promise in the purification of vehicle exhaust during cold-start.

4. Conclusions

Using a surfactant-template method, a series of mesostructured catalysts Co_3O_4–CeO_2 were successfully prepared, which possess higher specific surface area and oxidation activity than the catalysts prepared by other methods. In these catalysts, Co_3O_4 crystallites are considered to be encapsulated by nano-sized CeO_2, with only a small fraction of Co ions exposing on the surface and strongly interacting with CeO_2. Such a structure maximizes the interaction between Co_3O_4 and CeO_2 in three dimensions. As a result, the reduction of Co_3O_4 to Co^{2+} is promoted by lengthening of Co–O bond at interface; and the oxidation of metallic Co to Co_3O_4 is also promoted by the easier oxygen supply from CeO_2; in addition, the reduction of Co^{2+} to metallic Co is remarkably delayed by the stabilization effect of CeO_2 and the absence of hydrogen spillover. After deposition of Pd, both the reduction and oxidation of cobalt phases are promoted to a great extent due to hydrogen or oxygen spillover effects.

The oxidation activity of these catalysts does not increase with the surface cobalt concentration increasing, but exhibit a volcano-type pattern. Co_3O_4–CeO_2 is highly active in adsorbing CO as bidentate carbonates, which serve as the intermediates for CO oxidation. Over Co_3O_4–CeO_2, the CO oxidation should take place preferentially at the interface between Co_3O_4 and CeO_2, and the oxidation-assisted creation of oxygen vacancies is regarded as the rate-determining step. O_2-TPD results reveal that the oxidation performance correlates very well with the amount of surface oxygen vacancies. Hence, the highest oxidation activity of the catalyst with Co/(Co + Ce) atomic ratio of 30% is originated from the largest amount of oxygen vacancies. With the addition of a small amount of Pd to this catalyst, a markedly improved activity for CO oxidation is achieved even at room temperature, much better than those of Co_3O_4–CeO_2 and Pd/CeO_2. A synergy effect between Pd and Co_3O_4–CeO_2 is responsible for this activity enhancement. A novel and different reaction pathway is proposed, namely Co_3O_4–CeO_2 phase adsorbs CO as bidentate carbonates and Pd phase activates the molecular oxygen. The activated oxygen atoms are rather mobile and reactive, readily reacting with the adsorbed CO through spillover. Therefore, oxygen vacancies are no longer required during reaction, leading to the decreased activation energy and improved catalytic performance of this catalyst.

Acknowledgments

This work is financially supported by the "863 Program" of the Ministry of Science & Technology of China (No. 2006AA06Z348), the National Natural Science Foundation of China (No. 20676097), the Natural Science Foundation of Tianjin (No. 05YFJMJC09700) and the Specialized Research Fund for the Doctoral Program of Higher Education of China (No. 20040056028). The authors are also grateful to the support of the Program for New Century Excellent Talents in University of China (NCET 07-0599), the Program for Introducing Talents of Discipline to University of China (No. B06006) and the Cheung Kong Scholar Program for Innovative Teams of the Ministry of Education (No. IRT0641).

Supporting material

Supporting material for this article may be found on ScienceDirect in the online version.

Please visit doi: 10.1016/j.jcat.2008.01.007.

References

[1] R. Westerholm, A. Christensen, Å. Rosén, Atmos. Environ. 30 (1996) 3529.
[2] J. Jansson, J. Catal. 194 (2000) 55.
[3] J. Jansson, A.E.C. Palmqvist, E. Fridell, M. Skoglundh, L. Österlund, P. Thormählen, V. Langer, J. Catal. 211 (2002) 387.
[4] P. Thormählen, M. Skoglundh, E. Fridell, B. Andersson, J. Catal. 188 (1999) 300.
[5] M. Kang, M.W. Song, C.H. Lee, Appl. Catal. A 251 (2003) 143.
[6] C.W. Tang, C.C. Kuo, M.C. Kuo, C.B. Wang, S.H. Chien, Appl. Catal. A 309 (2006) 37.
[7] M.M. Natile, A. Glisenti, Chem. Mater. 17 (2005) 3403.
[8] L.F. Liotta, G. Di Carlo, G. Pantaleo, A.M. Venezia, G. Deganello, Appl. Catal. B 66 (2006) 217.
[9] L.F. Liotta, G. Di Carlo, G. Pantaleo, G. Deganello, Appl. Catal. B 70 (2007) 314.

[10] P.G. Harrison, I.K. Ball, W. Daniell, P. Lukinskas, M. Céspedes, E.E. Miró, M.A. Ulla, Chem. Eng. J. 95 (2003) 47.
[11] L. Xue, C. Zhang, H. He, Y. Teraoka, Appl. Catal. B 75 (2007) 167.
[12] L. Spadaro, F. Arena, M.L. Granados, M. Ojeda, J.L.G. Fierro, F. Frusteri, J. Catal. 234 (2005) 451.
[13] J.Y. Luo, M. Meng, Y. Qian, Z.Q. Zou, Y.N. Xie, T.D. Hu, T. Liu, J. Zhang, Catal. Lett. 116 (2007) 50.
[14] Z.Q. Zou, M. Meng, J.Y. Luo, Y.Q. Zha, Y.N. Xie, T.D. Hu, T. Liu, J. Mol. Catal. A 249 (2006) 240.
[15] M.F. Luo, J.M. Ma, J.Q. Lu, Y.P. Song, Y.J. Wang, J. Catal. 246 (2007) 52.
[16] S. Golunski, R. Rajaram, CATTECH 6 (2002) 30.
[17] M. Fernández-García, A. Martínez-Arias, A. Iglesias-Juez, A.B. Hungría, J.A. Anderson, J.C. Conesa, J. Soria, J. Catal. 214 (2003) 220.
[18] A.B. Hungría, A. Iglesias-Juez, A. Martínez-Arias, M. Fernández-García, J.A. Anderson, J.C. Conesa, J. Soria, J. Catal. 206 (2002) 281.
[19] Y.J. Mergler, A. Van Aalst, J. Van Delft, B.E. Nieuwenhuys, Appl. Catal. B 10 (1996) 245.
[20] M. Meng, Y.Q. Zha, J.Y. Luo, T.D. Hu, Y.N. Xie, T. Liu, J. Zhang, Appl. Catal. A 301 (2006) 145.
[21] Y. Bi, L. Chen, G. Lu, J. Mol. Catal. A 266 (2006) 173.
[22] S.K. Kulshreshtha, M.M. Gadgil, Appl. Catal. B 11 (1997) 291.
[23] L.F. Liotta, G. Di Carlo, G. Pantaleo, A.M. Venezia, G. Deganello, E. Merlone Borla, M. Pidria, Appl. Catal. B 75 (2007) 182.
[24] G.B. Hoflund, Z. Li, Appl. Surf. Sci. 253 (2006) 2830.
[25] J. Łojewska, A. Kołodziej, J. Żak, J. Stoch, Catal. Today 105 (2005) 655.
[26] L.F. Liotta, G. Di Carlo, G. Pantaleo, G. Deganello, E. Merlone Borla, M. Pidria, Catal. Commun. 8 (2007) 299.
[27] K.S.W. Sing, D.H. Everett, R.A.W. Haul, L. Moscou, R.A. Pierotti, J. Rouquérol, T. Siemieniewska, Pure Appl. Chem. 57 (1985) 603.
[28] A. Martínez-Arias, A.B. Hungría, M. Fernández-García, J.C. Conesa, G. Munuera, J. Phys. Chem. B 108 (2004) 17983.
[29] M.S. Batista, R.K.S. Santos, E.M. Assaf, J.M. Assaf, E.A. Ticianelli, J. Power Sources 134 (2004) 27.
[30] F. Morales, D. Grandjean, A. Mens, F.M.F. de Groot, B.M. Weckhuysen, J. Phys. Chem. B 110 (2006) 8626.
[31] O.V. Komova, A.V. Simakov, V.A. Rogov, D.I. Kochubei, G.V. Odegova, V.V. Kriventsov, E.A. Paukshtis, V.A. Ushakov, N.N. Sazonova, T.A. Nikoro, J. Mol. Catal. A 161 (2000) 191.
[32] J.R. Chang, S.L. Chang, T.B. Lin, J. Catal. 169 (1997) 338.
[33] H.C. Yao, Y.F.Y. Yao, J. Catal. 86 (1984) 254.
[34] P. Arnoldy, J.A. Moulijn, J. Catal. 93 (1985) 38.
[35] A. Martínez-Arias, M. Fernández-García, O. Gálvez, J.M. Coronado, J.A. Anderson, J.C. Conesa, J. Soria, G. Munuera, J. Catal. 195 (2000) 207.
[36] W. Gac, Appl. Catal. B 75 (2007) 107.
[37] C.M.Y. Yeung, K.M.K. Yu, Q.J. Fu, D. Thompsett, M.I. Petch, S.C. Tsang, J. Am. Chem. Soc. 127 (2005) 18010.
[38] Z. Liu, J. Hao, L. Fu, T. Zhu, Appl. Catal. B 44 (2003) 355.
[39] D.V. Cesar, C.A. Peréz, M. Schmal, V.M.M. Salim, Appl. Surf. Sci. 157 (2000) 159.
[40] L.H. Chang, N. Sasirekha, Y.W. Chen, W.J. Wang, Ind. Eng. Chem. Res. 45 (2006) 4927.
[41] P. Dutta, S. Pal, M.S. Seehra, Y. Shi, E.M. Eyring, R.D. Ernst, Chem. Mater. 18 (2006) 5144.
[42] S. Kaliaguine, A. Van Neste, V. Szabo, J.E. Gallot, M. Bassir, R. Muzychuk, Appl. Catal. A 209 (2001) 345.
[43] S. Royer, D. Duprez, S. Kaliaguine, Catal. Today 112 (2006) 99.
[44] H.K. Lin, C.B. Wang, H.C. Chiu, S.H. Chien, Catal. Lett. 86 (2003) 63.
[45] J. Jansson, M. Skoglundh, E. Fridell, P. Thormählen, Top. Catal. 16/17 (2001) 385.
[46] O. Pozdnyakova, D. Teschner, A. Wootsch, J. Kröhnert, B. Steinhauer, H. Sauer, L. Toth, F.C. Jentoft, A. Knop-Gericke, Z. Paál, R. Schlögl, J. Catal. 237 (2006) 17.
[47] V. Shapovalov, H. Metiu, J. Catal. 245 (2007) 205.
[48] G. Sedmak, S. Hočevar, J. Levec, J. Catal. 213 (2003) 135.
[49] J.B. Wang, D.H. Tsai, T.J. Huang, J. Catal. 208 (2002) 370.
[50] B. Białobok, J. Trawczyński, W. Miśta, M. Zawadzki, Appl. Catal. B 72 (2007) 395.
[51] T. Nowitzki, A.F. Carlsson, O. Martynov, M. Naschitzki, V. Zielasek, T. Risse, M. Schmal, H.-J. Freund, M. Bäumer, J. Phys. Chem. C 111 (2007) 8566.
[52] G. Glaspell, L. Fuoco, M.S. El-Shall, J. Phys. Chem. B 109 (2005) 17350.
[53] P. Bera, K.C. Patil, V. Jayaram, G.N. Subbanna, M.S. Hegde, J. Catal. 196 (2000) 293.
[54] T. Schalow, B. Brandt, M. Laurin, S. Schauermann, J. Libuda, H.-J. Freund, J. Catal. 242 (2006) 58.
[55] H. Zhu, Z. Qin, W. Shan, W. Shen, J. Wang, J. Catal. 233 (2005) 41.